AGU PUBLICATIONS

JGR

Journal of Geophysical Research: Oceans

RESEARCH ARTICLE

10.1002/2014JC010328

Key Points:
- In situ and satellite-based wind differences affect whitecap fraction estimates
- Whitecap fraction parameterizations should be updated for satellite-based winds
- Discrepancies exist between visible and radiometric whitecap observations

Correspondence to:
A. C. Paget,
aaroncpaget@gmail.com

Citation:
Paget, A. C., M. A. Bourassa, and M. D. Anguelova (2015), Comparing in situ and satellite-based parameterizations of oceanic whitecaps, *J. Geophys. Res. Oceans*, *120*, 2826–2843, doi:10.1002/2014JC010328.

Received 22 JUL 2014
Accepted 24 MAR 2015
Accepted article online 3 APR 2015
Published online 11 APR 2015

Comparing in situ and satellite-based parameterizations of oceanic whitecaps

Aaron C. Paget[1,2], Mark A. Bourassa[2], and Magdalena D. Anguelova[3]

[1]Microwave Earth Remote Sensing Laboratory, Brigham Young University, Provo, Utah, USA, [2]Department of Earth, Ocean, and Atmospheric Science and Center for Ocean-Atmospheric Prediction Studies, Florida State University, Tallahassee, Florida, USA, [3]Remote Sensing Division, Naval Research Laboratory, Washington, District of Columbia, USA

Abstract The majority of the parameterizations developed to estimate whitecap fraction uses a stability-dependent 10 m wind (U_{10}) measured in situ, but recent efforts to use satellite-reported equivalent neutral winds (U_{10EN}) to estimate whitecap fraction with the same parameterizations introduce additional error. This study identifies and quantifies the differences in whitecap parameterizations caused by U_{10} and U_{10EN} for the active and total whitecap fractions. New power law coefficients are presented for both U_{10} and U_{10EN} parameterizations based on available in situ whitecap observations. One-way analysis of variance (ANOVA) tests are performed on the residuals of the whitecap parameterizations and the whitecap observations and identify that parameterizations in terms of U_{10} and U_{10EN} perform similarly. The parameterizations are also tested against the satellite-based WindSat Whitecap Database to assess differences. The improved understanding aids in estimating whitecap fraction globally using satellite products and in determining the global effects of whitecaps on air-sea processes and remote sensing of the surface.

1. Introduction

For the last 50 years, scientists have studied the fraction of the world's oceans covered by whitecaps in an attempt to relate this fraction to some other readily measureable quantities, such as wind speed. Functions derived from these measurable quantities are used for estimating the whitecap fraction locally and globally, and then these estimates are used to determine the onset of wave breaking [*Blanchard*, 1963; *Williams*, 1969; *Monahan et al.*, 1983; *Monahan and O'Muircheartaigh*, 1986], the effects of whitecaps on satellite surface measurements [*Wentz*, 1983, 1997; *Gordon and Wang*, 1994; *Smith*, 1988; *Gordon and Voss*, 1999; *Rose et al.*, 2002; *Anguelova and Webster*, 2006], and geophysical processes such as surface albedo, sea spray production, and CO_2 exchange [*Blanchard*, 1983; *Woolf*, 1997; *Haywood et al.*, 1999; *de Leeuw et al.*, 2011]. Improved understanding and quantification of air-sea processes and surface fluxes associated with whitecaps requires a better understanding of the nature of the errors and reduction of errors of whitecap fraction estimates.

Whitecaps are conspicuous manifestations of wave breaking. The air entrained into the water by breaking waves forms a cloud of bubbles with a wide range of sizes [*Deane and Stokes*, 2002; *Lewis and Schwartz*, 2004; *de Leeuw et al.*, 2011]. The smallest bubbles (radii < 100 μm) quickly dissolve and disappear [*Thorpe*, 1982; *Memery and Merlivat*, 1985; *Woolf and Thorpe*, 1991], while larger and more buoyant bubbles rise to the surface forming and constantly replenishing floating bubble rafts. Both the subsurface bubble clouds (also called bubble plumes) and the foam floating on the surface constitute whitecaps. Whitecap fraction W quantifies the surface extent of the whitecaps.

The surface part of the whitecaps bears further distinction. At the moment of active breaking (when the air is forced into the water), the active breaking whitecaps are visually bright and highly reflective. These whitecaps sit at and travel with the wave crest, and cover a small portion of the total bubble-covered surface area. These actively generated whitecaps are referred to as stage A (young) whitecaps [*Monahan and Woolf*, 1989], and active whitecap fraction W_A quantifies their spatial extent. These whitecaps are usually thicker than 1 cm vertically at the surface [*Anguelova and Gaiser*, 2011]. Whitecaps evolve fast and after the breaking event transition quickly to stage B (mature) whitecaps which comprise decaying foam and froth formed by the bubbles rising from below. In contrast to the active whitecaps, these residual whitecaps are thinner vertically and less bright, linger behind the wave that has created them, and spread over a larger area; residual whitecap fraction W_B quantifies their areal coverage.

Active and residual whitecaps are associated with different processes that take place at the air-sea interface. More dynamic processes such as momentum transfer, energy dissipation, turbulent mixing, gas exchange, and production of spume drops are better parameterized in terms of W_A [*Melville*, 1996; *Asher et al*., 1998; *Melville and Matusov*, 2002; *Andreas et al*., 2008]. The total whitecap fraction $W = W_A + W_B$ is important for bubble-mediated production of sea spray and heat exchange [*Andreas et al*., 2008; *de Leeuw et al*., 2011]. Because W_A and W_B can differ by more than a factor of 10 depending on the wind conditions [*Monahan and Woolf*, 1989], it is important to parameterize the various air-sea processes in terms of the most suitable quantity W_A, W_B, or W. In the published literature, whitecap fraction W representing both types of whitecaps is usually reported, unless specific effort to represent either W_A or W_B is stated.

Historically, whitecap fraction was estimated as a function of the 10 m wind speed, U_{10}, a frequently recorded variable. Although various types of functions have been used [*Monahan*, 1971; *Wilheit*, 1979; *Bondur and Sharkov*, 1982; *Monahan and O'Muircheartaigh*, 1986; *Monahan*, 1993], the power law has been the predominant choice for parameterizing the $W(U_{10})$ relationship

$$W = aU_{10}^{b}, \tag{1}$$

where a and b are coefficients. Using in situ W and U_{10} data, each new $W(U_{10})$ parameterization gives values of a and b representative for a given in situ data set collected at meteorological and oceanographic conditions specific for the location of the field campaign. This leads to multiple problems when parameterizations based on in situ W and U_{10} data are used to provide air-sea fluxes on a global scale for climate and geophysical models [*de Leeuw et al*., 2011]. One problem of using locally derived $W(U_{10})$ parameterizations globally is that such parameterizations are combined with global fields of wind speed obtained from satellite-based instruments without examining how the principle and accuracy of measuring U_{10} with different techniques affect the values of coefficients a and b in (1). Satellite-based measurements can provide consistent measurements for long-term studies for specific locations over specific time periods more easily than traditional ship-based studies, and data are already largely available for use in research.

Only recently has this problem been addressed [*Goddijn-Murphy et al*., 2011; *Salisbury et al*., 2013, 2014]. *Goddijn-Murphy et al*. [2011] examined the performance of many $W(U_{10})$ parameterizations by using the in situ W data set of *Callaghan et al*. [2008] with wind speeds from different sources, namely ship-based winds from Marine Aerosol Production (MAP) campaign, satellite-based winds from the SeaWinds scatterometer on QuikSCAT, and wind data from the European Center for Medium range Weather Forecasting (ECMWF). As expected, *Goddijn-Murphy et al*. [2011] found that all $W(U_{10})$ parameterizations performed better when coupled with in situ wind speeds than with satellite-based or modeled wind speeds. Their study confirmed that the power law coefficients a and b in (1) vary not only with the location and specific experimental conditions but also with the source of wind speed data. However, it has still not been determined how the coefficients a and b in (1) might vary if one considers the fact that satellites (e.g., QuikSCAT) provide equivalent neutral wind, U_{10EN}, which is more analogous to a stress and accounts for the atmospheric stability effects on the wind profile [*Kara et al*., 2008] while the in situ U_{10} values are usually not adjusted for stability effects.

A likely problem of using locally derived $W(U_{10})$ parameterizations on a global scale is that they cannot be expected to model adequately the variability of W caused by variations of meteorological and oceanographic conditions from one location to another over the globe. To develop $W(U_{10})$ parameterizations applicable for different geographical locations, one needs W values obtained over wide range of conditions. *Anguelova and Webster* [2006, Table 2] showed that a database compiled of existing data sets for W is limited in representing a wide range of conditions, unevenly representing the parameter space; this leads to underrepresentation of whitecap fraction over vast expanses of the open ocean. To build a database of W values which contain the natural variability of whitecaps, *Anguelova and Webster* [2006] developed a method to obtain whitecap fraction from satellite observations of the brightness temperature T_B of the ocean surface at microwave frequencies. Besides capturing geographical and seasonal variability, satellite-based estimates of whitecap fraction at different radiometric frequencies W_f, where f denotes the frequency, can represent (at least to some extent) differences in the variability of predominantly active whitecaps and active plus residual whitecaps.

Salisbury et al. [2013] investigated the variability of whitecap fraction as a function of different forcing factors using a year-long global database of satellite-based W_f values referred to here as WindSat Whitecap Database (WWD). They also demonstrated the expected substantial differences in W_f variability at different

Table 1. List of Names and Descriptions of the Variables Used in This Study

Variable Name	Description
U_{10}	Stability-dependent in situ 10 m wind speed
U_{10EN}	Ten meter equivalent neutral wind speed, used generically or as identified in the text
U_{10ENi}	Stability-independent adjusted in situ 10 m equivalent neutral wind speed
U_{10ENs}	Satellite 10 m equivalent neutral wind speed
W	In situ total whitecap fraction observations
W_A	In situ stage A whitecap fraction observations
W_i	Total whitecap fraction parameterization optimized with U_{10}
W_{ENi}	Total whitecap fraction parameterization optimized with U_{10ENi}
W_{Ai}	Stage A whitecap fraction parameterization optimized with U_{10}
W_{AENi}	Stage A whitecap fraction parameterization optimized with U_{10ENi}
W_{10}	Whitecap fraction from the WindSat 10 GHz channel of the WWD, closely related to stage A whitecap fraction
W_{37}	Whitecap fraction from the WindSat 37 GHz channel of the WWD, closely related to total whitecap fraction

frequencies, or, equivalently, different relative presence of active and residual whitecaps. *Monahan and O'Muircheartaigh* [1986] contend that atmospheric stability affects W from in situ observations. *Salisbury et al*. [2013] documented notable dependence of satellite-based W_f on atmospheric stability. They cautioned that it should not be expected that a parameterization W_f (U_{10EN}), based on satellite data for both whitecap fraction and wind speed, should exhibit the same wind speed/stress dependence on stability as $W(U_{10})$ based on in situ measurements. However, differences between $W(U_{10})$ and W_f (U_{10EN}) were not quantified.

Satellite winds (U_{10EN}) and in situ winds (U_{10}), though both reported at a height of 10 m, are not the same. The in situ wind, considered a true wind, is Earth relative and responds to the effects of stability in the atmospheric boundary layer as modeled with traditional boundary layer wind profiles. Satellite winds are based on stability-dependent stresses (and roughness lengths) used to neutrally adjust the winds to 10 m. That is, satellite winds are given assuming an equivalent neutral profile consistent with the parameterized stress [*Tang and Liu*, 1996]. Satellite winds and in situ winds can be related when the atmospheric stability is known, and mean surface motion is known or ignored [*Kara et al*., 2008].

To study the effects of the different types of wind on whitecap parameterizations, the stability-dependent in situ wind measured at 10 m, U_{10}, and the stability-independent equivalent neutral wind, U_{10EN}, are used to develop new whitecap parameterizations for W and W_A. The U_{10EN} values that are calculated from in situ sources are identified as U_{10ENi}, and the U_{10EN} values that come from satellite sources are identified as U_{10ENs}. Whitecap parameterizations for W and W_A optimized using U_{10} are identified by the symbols W_i and W_{Ai}, respectively; the whitecap parameterizations for W and W_A optimized using U_{10ENi} are identified by the symbols W_{ENi} and W_{AENi}, respectively (Table 1). Combinations of the wind types and whitecap parameterizations are compared against other combinations, e.g., $W_{Ai}(U_{10})$ can be compared to $W_{AENi}(U_{10ENi})$.

The objective of this study is to identify and quantify differences between $W(U_{10})$ parameterizations for both active whitecap fraction W_A and total (active+residual) whitecap fraction W caused by (1) effects of applying stability adjusted in situ wind speeds on in situ whitecap fraction observations and (2) effects of applying these in situ-derived parameterization coefficients (for both stability-dependent and stability-adjusted winds) to in situ whitecap fraction observations combined with satellite-based winds speeds. Our approach is to first determine power law coefficients using available in situ whitecap observations W_A and W with in situ stability-dependent winds U_{10} and the in situ stability-adjusted U_{10}, U_{10ENi}. These new whitecap parameterizations $W_{Ai}(U_{10})$, $W_i(U_{10})$, $W_{AENi}(U_{10ENi})$, and $W_{ENi}(U_{10ENi})$ based solely on in situ data are compared against the corresponding in situ whitecap observations. Then, the parameterizations obtained with satellite-based winds U_{10ENs} in the argument—$W_{Ai}(U_{10ENs})$, $W_i(U_{10ENs})$, $W_{AENi}(U_{10ENs})$, and $W_{ENi}(U_{10ENs})$—are compared to W_f and U_{10ENs} from the WWD to assess differences.

2. Background

2.1. Whitecap Fraction From In Situ Observations

In situ observational studies of whitecaps have focused on relating the wind speed to the fraction of water covered by whitecaps. Observations have come from video, photography, visual inspection, and remote sensors from observing platforms, which include land, ship, pier, buoy, towers, aircraft, and satellites.

Observations have been collected around the globe and in many bodies of water during different field campaigns. Observations of whitecap fraction have been fit to functions using wind speed or other recorded quantities [*Monahan and O'Muircheartaigh*, 1986; *Goddijn-Murphy et al*., 2011].

To measure whitecaps with camera or video technique, a series of sequential observations are taken of the whitecap(s) and the surrounding area. These images resolve the shapes of the whitecaps against the nonwhitecap-covered area; sea spray and individual bubbles from whitecaps are not resolved. Various analysis approaches determine the ratio of the area containing whitecaps to the total area using brightness thresholds or other techniques [*Callaghan et al*., 2008, *Callaghan and White*, 2009]. Statistical uncertainty in determining the whitecap fraction is reduced by increasing the number of images included in calculating the whitecap fraction. Although a number of techniques are available to calculate whitecap fraction, typically only one technique is applied for the observations from each campaign or series of sequential observations.

For photographs or digital still images, the whitecap fraction values, statistical by nature, from each set of the sequential series of individual images are averaged to record one data point. The number of images used in each average varies from as little as five [*Monahan et al*., 1984] to thousands [*Callaghan et al*., 2008] of individual images and depends on the technique, number of available images, and time frame. Whitecaps may become statistically different after 3–4 s [*Callaghan et al*., 2012; *Callaghan*, 2013]; the minimum recommended sampling frequency is 0.25–0.33 Hz to achieve a consistent 5% statistical uncertainty for each W data point [*Callaghan et al*., 2008; *Callaghan and White*, 2009]. Oversampling does not provide truly independent measures of W, but image contamination from glint, sky reflection, raindrops, and other effects can reduce the number of images and the sampling frequency of the images used to determine one data point. Historical data sets probably undersampled the ocean surface according to these modern standards; however, the efforts given in the observing, processing, and publication of these data sets should be lauded. These early efforts provided the basis for the understanding and methodologies we employ today.

From the processed images, each averaged value is reported as an individual whitecap observation and the individual whitecap observations are paired with the corresponding wind, temperature, and other recorded information. *Anguelova and Webster* [2006] summarize data sets developed with this approach. Uncertainties in whitecap fraction values are reduced with an increase in the number of images used to determine those values; *Callaghan and White* [2009] showed that on the order of hundreds of images should be averaged to achieve convergent values for one W data point. As a result, uncertainties are not consistent across all data set.

Techniques used to determine the active whitecap fraction W_A include an intensity threshold [*Asher et al*., 1998], the breaking crest length distribution $\Lambda(c)$ (with c being the breaking velocity) coupled with a time scale [*Kleiss and Melville*, 2011], or a combination of the intensity threshold approach with considerations of kinematic properties and breaking wave temporal evolution [*Mironov and Dulov*, 2008]. Calibration between different techniques has not been pursued, but the basic principles of discriminating whitecaps against the surrounding water remain the same regardless of the method of calculation. Because of this, the observations can be compared with the caveat that the techniques are expected to have unique biases.

Empirical parameterizations are derived using individual data sets, portions of data sets, or medleys of data sets. *Wu* [1979, 1988, 1992] suggested that theoretically whitecap fraction follows a power law based on the wind speed cubed (and multiplied by a wind speed dependent drag coefficient, which is effectively the wind speed raised to the 3.75 power [*Monahan and O'Muircheartaigh*, 1982]). This suggestion has fueled some of the known parameterizations for determining whitecap fraction [*Anguelova and Webster*, 2006, Table 1]. Altogether, over 260 different parameterizations have been identified in the literature [*Monahan and O'Muircheartaigh*, 2012].

Values of U_{10} from in situ observation data sets typically ranged from 0 through 25 m s^{-1}. Wind speeds in excess of 25 m s^{-1} account for less than 2% of the global wind speed distribution [*Salisbury et al*., 2013]. The majority of in situ observations were for wind speeds below 12 m s^{-1}; difficulties arise in making in situ observations at higher wind speeds as the wind conditions are increasingly scarce. Though new data sets extend the range of U_{10} above 15 m s^{-1} [*Lafon et al*., 2004, 2007; *Callaghan et al*., 2008; *Mironov and Dulov*, 2008], the data used to derive the empirical parameterizations do not represent the full range of U_{10}. Additional observations are needed to reduce errors in the whitecap fraction estimates globally. *Anguelova and*

Table 2. Data Sets Contributing to the Combined Data Set of In Situ Measurements Used for This Study[a]

Source	Name in Plot Legends	W	W_A	Number of Values
Nordberg et al. [1971]	Nordberg71	X	X	4
Monahan [1971]	Monahan71	X		54
Ross and Cardone [1974]	RossCardone74	X	X	13
Monahan et al. [1983]	JASIN83	X		64
Doyle [1984]	STREX83	X		85
Monahan et al. [1984]	MIZEX83-film	X		21
Monahan et al. [1984]	MIZEX83-video		X	29
Monahan et al. [1985]	MIZEX84-film	X		37
Monahan et al. [1985]	MIZEX84-video		X	60
Monahan et al. [1985]	HEXOS84		X	27
Sugihara et al. [2007]	Sugihara07	X		91
Callaghan et al. [2008]	MAP	X		44
Mironov and Dulov [2008]	MD08	X	X	71

[a]Sources, reported whitecap type, and number of contributing values are shown.

Webster [2006] compiled a database of historical observations, now updated from 1971 to 2010, for active W_A, residual W_B, and total W whitecap fractions with their time, location, and available geophysical attributes. The historical database provides observations over a wide range of wind speeds in multiple global locations and under different atmospheric conditions.

2.2. Whitecap Fraction Using Satellite Wind Speeds

One source of error is using incongruent type of wind data in the parameterizations to estimate whitecap fraction, i.e., using satellite-based instead of in situ winds. Much like using a 2 m wind to estimate whitecap fraction with a parameterization developed with a 10 m wind introduces unnecessary errors in the whitecap estimation, using satellite-based winds that are surface relative in parameterizations optimized for in situ winds that are earth-relative also introduces errors. Most of the parameterizations depend on U_{10} and follow some form of a power law, but they were not developed for use with satellite-based winds. Satellite-based winds, which are reported as equivalent neutral 10 m winds U_{10EN}, differ from U_{10} winds [*Kara et al.*, 2008; *May and Bourassa*, 2011; *Plagge et al.*, 2012]. Satellite winds are tuned to produce the correct stress when combined with a neutral drag coefficient. Applying U_{10EN} to whitecap functions well trained on U_{10} increases the error of the whitecap fraction estimates.

In situ measured wind speed is typically the time average (often 10 min) wind speed for a single point measurement, adjusted to a 10 m height if necessary, and can be taken in a single location continuously; satellite-based wind speed are an area-averaged wind speed based on surface roughness characteristics from the satellite footprint (or multiple footprints) on the ocean surface [*May and Bourassa*, 2011] (e.g., 24 km $\times$ 31 km ellipse at inner beam for QuikSCAT [*Bartsch*, 2010]). Satellites make instantaneous observations of the earth's surface but must complete at least one orbit before observing a given area again; normally a given location is only observed at most twice daily, but can provide global coverage. In situ observations can be continuously made for a single location over long periods of time. The similarity between in situ and satellite observations can be improved [*May and Bourassa*, 2011] by using frozen turbulence theory proposed by *Taylor* [1938], provided that high temporal resolution in situ data are available.

Converting in situ U_{10} observations to U_{10EN} is possible using an air temperature T_{air} and sea surface temperature T_s differential dT, such that $dT = T_{air} - T_s$ where $dT > 0$ (<0) indicates stable (unstable) atmospheric conditions, and an estimate of sea state and the surface motion (e.g., swell, orbital velocity, and currents) [*Kara et al.*, 2008]. In situ observations of U_{10} and dT with corresponding W and W_A whitecap observations already exist (Table 2), as do satellite-based observations of U_{10EN} and whitecaps [*Anguelova and Webster*, 2006].

Satellite observations are a valuable source of global wind speed fields, but the differences between satellite U_{10EN} and in situ U_{10} have to be appreciated (Figure 1) in the context of whitecaps. Atmospheric stability plays a role in the difference between U_{10} and U_{10EN} by affecting the drag coefficient and the wind speed vertical profile [*Kara et al.*, 2005, 2008]. The effects of stability on the vertical wind profile are largely accounted for with U_{10EN}. Stability is modeled in terms of a buoyancy-related mixing which usually dominates for lower wind speeds and mechanical mixing that often dominates for higher wind speeds [*Kara*

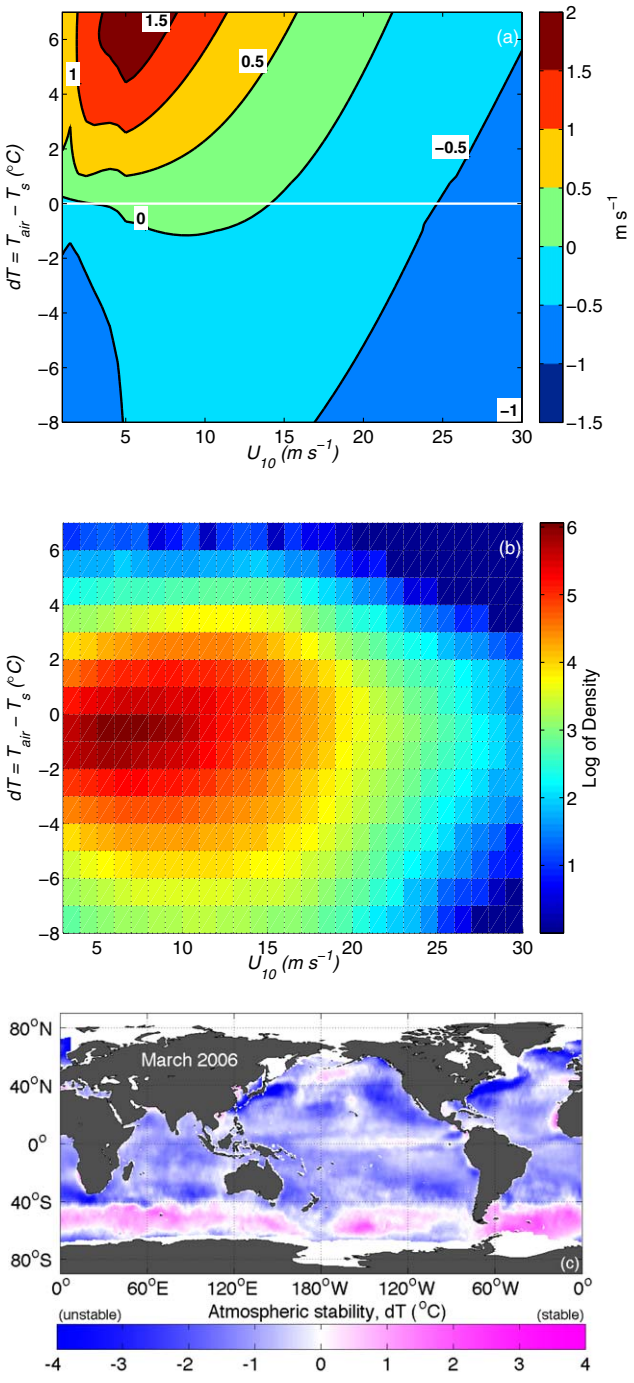

Figure 1. (a) The differences between U_{10} and U_{10EN} after U_{10} was converted to U_{10EN} using equations from *Kara et al.* [2005] for $-8°C < dT < 7°C$ and over the range of $1 < U_{10} < 40$ m s^{-1}. (b) The distribution of wind speed and stability globally from the WindSat Whitecap Database for $-8°C < dT < 7°C$ and over the range of $3 < U_{10} < 30$ m s^{-1}. (c) Global map of dT for March 2006.

et al., 2008]. Buoyancy-related mixing causes departures from a neutral log-profile and hence the stability-related difference between U_{10} and U_{10EN}. Mechanical mixing reduces the impact of buoyancy-related mixing, thereby reducing differences between U_{10} and U_{10EN}. For example, U_{10} with a value of 5 m s^{-1} and $dT > 5°C$ is over 1.5 m s^{-1} greater than U_{10EN} for the same conditions, a 30% or greater difference in wind speed according to *Kara et al.* [2008]. Over the wind speed ranges commonly found in the atmosphere ($U_{10} < 26$ m s^{-1}), the difference between U_{10} and U_{10EN} varies between −0.75 and 1.8 m s^{-1}.

While whitecaps are often related to a 10 m wind speed, atmospheric stability affects the surface interactions that help create whitecaps [*Anguelova and Webster*, 2006]. For example, under unstable atmospheric conditions, a 10 m wind of 3 m s^{-1} can generate whitecaps, but under stable atmospheric conditions, a 10 m wind of 6 m s^{-1} might not generate any whitecaps [*Monahan and O'Muircheartaigh*, 1986; *Stramska and Petelski*, 2003]. The wind near the surface imparts stress to the ocean surface and contributes to whitecap formation. The stress can be described by the 10 m wind speed, but only with atmospheric stability and sea surface conditions. The surface stress, however, is directly related to U_{10EN}. Though implicitly, the use of U_{10EN} helps to account for the effects of atmospheric stability on whitecap formation.

Even the small differences between the in situ and satellite wind speeds make large differences in the whitecap estimates because of the nonlinearity of the $W(U_{10})$ relationship. Using U_{10EN} in parameterizations developed for U_{10} introduces errors in whitecap estimates. For example, using the whitecap parameterization $W = 3.84 \times 10^{-6} U_{10}^{3.41}$ [*Monahan and O'Muircheartaigh*, 1980] for $dT = -6°C$ and $U_{10} = 29$ m s^{-1}, $W(U_{10})$ gives a whitecap fraction of 0.41 and $W(U_{10EN})$ gives a whitecap fraction of 0.37, a difference of 0.04 in whitecap fraction or roughly 10% overestimation if using U_{10EN} in an equation developed for U_{10} (Figure 2). Converting U_{10EN} to U_{10} is possible and might be usable in U_{10}-based whitecap parameterizations, but the conversion is difficult without knowing a priori the atmospheric stability and the surface conditions, often unknown from satellite observations of U_{10EN}. Whitecap data sets with in situ observations of U_{10} and stability are available, though, and can be converted to U_{10EN}.

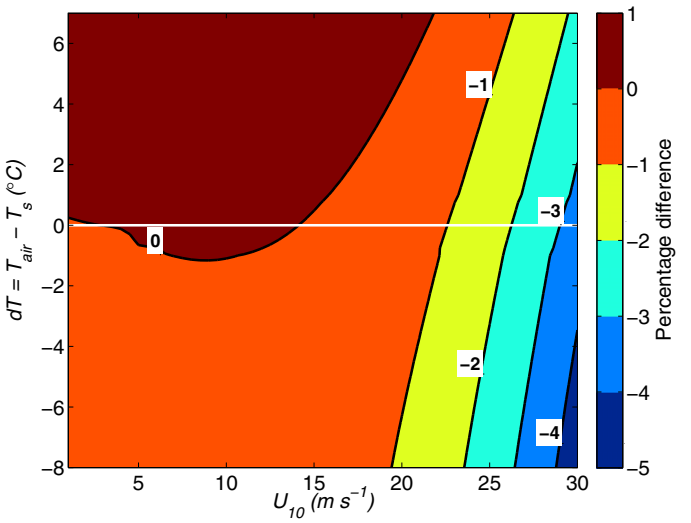

Figure 2. The differences between the percentage of whitecap fraction, $W(U_{10})$ minus $W(U_{10EN})$ [*Kara et al.*, 2005] for $-8°C < dT < 7°C$ and over the range of $1 < U_{10} < 30$ m s^{-1} using the parameterization for whitecap fraction $W = 3.84 \times 10^{-4}\, U_{10}^{3.41}$ (in percent) [*Monahan and O'Muircheartaigh*, 1980].

Developing new whitecap parameterizations based on U_{10EN} is a simpler solution to account for the natural variability of whitecapping and does not initially require the additional information of other geophysical parameters. Having a simple solution has merit since the addition of more variables could introduce unforeseen uncertainties in estimates of whitecap fraction. Whitecap parameterizations based on U_{10EN} can be determined from whitecap observations paired with U_{10EN} values from satellites [*Goddijn-Murphy et al.*, 2011; *Salisbury et al.*, 2013] or, as done in this study, by using historical whitecap observation data sets with the necessary geophysical information to convert U_{10} to U_{10EN}. These new U_{10EN} parameterizations can be compared to other whitecap-U_{10EN} observations for future analysis. While it would be valuable to analyze other geophysical parameters such as surfactants, salinity, and wave-current interactions, the in situ data used in this study does not include such information. Additionally, the impacts of various whitecap detection techniques, the temporal averaging of the wind, and various power law optimization techniques cannot be adequately explored with the available in situ data. Such studies require a large number of observations for a thorough analysis.

2.3. Whitecap Fraction From Satellite Observations

Satellite-based observations of whitecaps provide long-term, consistent global observations useful in estimating and studying whitecap fraction. *Anguelova et al.* [2006] and *Salisbury et al.* [2013, section 3] describe the algorithm estimating whitecap fraction from satellite observations W_f. Briefly, passive microwave observations can be used to determine W_f on the ocean surface using the emissivity properties of the sea foam comprising whitecaps. Changes in ocean surface emissivity due to presence of whitecaps are recorded as changes of brightness temperature, T_B. Whitecap fraction was calculated using WindSat observations of T_B [*Gaiser et al.*, 2004] and models [*Bettenhausen et al.*, 2006; *Anguelova and Gaiser*, 2013] which were run with input data for wind speed and direction, sea surface temperature, water vapor, cloud liquid water, and a constant salinity.

The microwave channels at 10 and 37 GHz respond differently to foam of different thicknesses [*Anguelova and Gaiser*, 2011]. Satellite-based whitecap fraction W_f at these frequencies, referred hereafter as W_{10} and W_{37} for f = 10 or 37 GHz, respond to different characteristics of the whitecaps (active whitecap fraction and total whitecap fraction, respectively). That is, W_{10} is a measure of predominantly active whitecaps and includes only partially residual whitecaps; though minor differences exist, W_{10} is comparable to W_A. Whitecap fraction W_{37} is a measure of the total, active plus residual, whitecap fraction and is thus comparable to W. *Salisbury et al.* [2013] parameterized W_{10} and W_{37} as a function of U_{10EN} up to 20 m s^{-1} from satellite observations.

Satellite-based W_f values do not resolve individual whitecaps; rather, the whitecap signal spatially averaged over the satellite footprint is obtained. The spatially averaged satellite whitecap observations have to be compared to temporally averaged in situ whitecap observations following principles proposed by *Taylor* [1938] and demonstrated by *Ichoku et al.* [2002]. In this sense, in situ W values obtained by averaging a number of sequential images of sea state (section 2.1) and satellite W_f values are reasonably comparable.

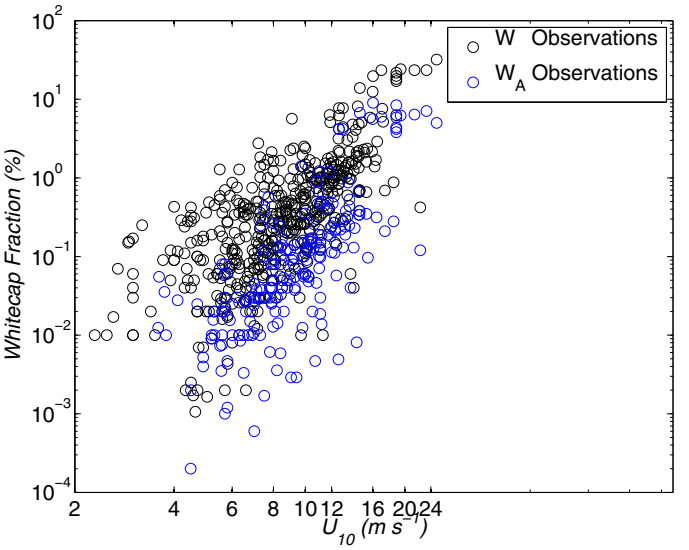

Figure 3. Whitecap observations from in situ data sets listed in Table 2. Both W_A and W with the respective U_{10}.

3. Data

3.1. In Situ Whitecap Data

A combined data set compiled specifically for this study pools together 13 of the available data sets (Table 2). These data sets are chosen because they contain the information necessary for converting U_{10} to U_{10EN} for comparison with satellite winds, i.e., the 204 (484) observations of W_A (W) include U_{10} and dT, or T_s and T_{air} for calculating dT. Only non-null whitecap observations are included in this analysis to maintain consistency with historical analysis of the same data. The observations from these data sets also represent diverse locations and observational conditions which are necessary to understand whitecaps globally. Figure 3 shows W and W_A as a function of wind speed U_{10} for all the data sets in Table 2. A lower limit for the wind speed range of 3 m s^{-1} is enforced with an upper wind speed limit enforced by available observations, around 25 m s^{-1}. It is necessary to assume that the reported winds are surface-relative and measured at a 10 m height. The distribution of the data points is skewed toward the lower wind speed values; consistent across observation techniques and observation platforms, both in situ and satellite. The range of minimum to maximum W_A (W) values increases with increasing wind speed from about 0.05% (1%) whitecap fraction difference at low wind speeds to 8% (23%) at higher wind speeds (Figure 3). The wider range suggests that the spread of the data is due to increasing variability of W_A and W with increasing wind speed as well as with increasing wind variability at higher wind speeds. The increase of the data spread as wind speed increases is consistent with previous studies [*Callaghan et al.*, 2008; *Goddijn-Murphy et al.*, 2011].

3.2. Satellite-Based Whitecap Data

The WindSat Whitecap Database (WWD) [*Salisbury et al.*, 2013] used for this study is a daily 0.5° × 0.5° global gridded product for 2006. Values of W_{10} and W_{37} are available for both the ascending and descending passes of the WindSat instrument. This data set averages 5.66 × 10^4 and 5.75 × 10^4 data points daily for W_{10} and W_{37} (Figure 4), respectively, which is approximately 2 × 10^7 data points for W_{10} and W_{37} each during 2006. This is the first continuous global whitecap data set that covers all seasons and includes the additional parameters of U_{10ENs}, wind direction, T_s, T_{air}, significant wave height H_s, and peak wave period T_p. The fetch, the geophysical processes, and the sea state associated with coastal regions are not explicitly addressed with this data set.

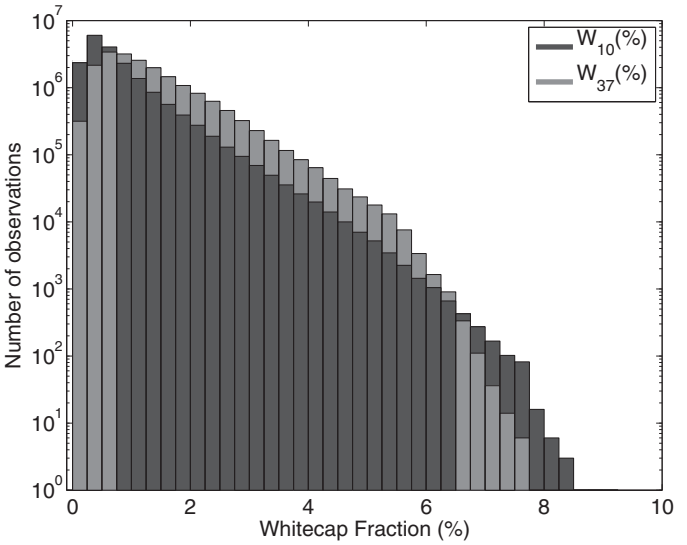

Figure 4. Histogram of whitecap fraction for W_{10} and W_{37} (in %) for the WindSat Whitecap Database.

The 10 m wind data from the WWD contains both the wind magnitude and the direction. The wind comes from QuikSCAT as equivalent neutral winds, U_{10ENs}, and when those are not available, from the Global Data Assimilation System (GDAS). WindSat winds are not used in the WWD and were not assimilated in GDAS during 2006. The official QuikSCAT performance is quoted at 3–25 m s^{-1} as better than 2 m s^{-1} (rms) [*Lungu and Callahan*, 2006; *Chang et al*., 2009]. Winds from GDAS are assumed to be similar, though the actual accuracy likely differs depending on the data used in the assimilation process. WindSat observations are collocated with wind data within ±60 min (for QuikSCAT) or ±180 min (for GDAS).

4. Methodology

4.1. Converting U_{10} to U_{10EN}

Various techniques are available to convert U_{10} to U_{10EN}; the technique used for this study was chosen on the basis of the available data. The conversion of in situ winds to equivalent neutral winds uses the actual wind (U), roughness length (z_0), friction velocity (U^*), von Karman constant ($k = 0.4$), drag coefficient (C_D), gravity ($g = 9.81$ m s^{-1}), and the Charnock constant ($\alpha = 0.015$)

$$U_{10EN} = \frac{U_*}{k} \ln\left(\frac{10}{z_0}\right), \tag{2}$$

$$U_* = U\sqrt{C_D}, \tag{3}$$

$$z_0 = \alpha \frac{U_*}{g}. \tag{4}$$

The Charnock constant is known to vary, but exactly how the constant changes is not well understood. Small changes in the choice of the Charnock constant do not strongly influence the calculated U_{10EN} because the consequences on the error are small compared to sampling related error. A nonconstant drag coefficient is used as suggested by *Powell et al*. [2003]. The drag coefficient is calculated using the formulas from *Kara et al*. [2005] and has a third-order dependence on U_{10} and a second-order dependence on dT. The drag coefficient equation is valid for U values from 1 to 40 m s^{-1} and dT values from −8 to 7°C and has the distinction of being continuous over the entire range of valid values. Through (2)–(4), U_{10} is adjusted to U_{10EN} and is thus directly comparable to satellite winds assuming zero mean surface motion since no observation-specific current and wave information is available. Surface motion could change U_{10EN} as much as 2 m s^{-1} faster or slower in regions of strong surface motion, but the actual change is likely less than 0.1 m s^{-1}.

Figure 1 shows the differences $U_{10} - U_{10EN}$ between stability-dependent U_{10} values and their adjusted U_{10EN} values over the range of $-8°C < dT < 7°C$ (representing over 98% of dT globally) and $1 < U_{10} < 40$ m s^{-1} as calculated from *Kara et al*. [2005] (observations greater than 26 m s^{-1} represent less than 0.02% of U_{10} globally). It is seen that in situ, stability-dependent winds could be up to 2 m s^{-1} higher than satellite-based, stability-adjusted winds for $U_{10} < 10$ m s^{-1}. The opposite is true for higher winds (above 15 m s^{-1}): the stability-dependent (in situ) winds could be lower than the stability-adjusted (satellite) by up to 1.5 m s^{-1}. Such differences are consistent with comparisons of U_{10} and their respective U_{10EN} given by *Kara et al*. [2008] and *Goddijn-Murphy et al*. [2011]. Figure 1b shows that over a year dT ranges mostly from −4 to +4°C (representing over 97.5% of all available observations). Extremely unstable conditions that can strongly affect W predictions are observed over warm currents like Kuroshio and Gulfstream in spring (Figure 1c), while overwhelming stable conditions characterize almost entirely the Southern ocean. March exemplifies the extreme dT values in these regions; the spatial distribution of dT changes throughout the year. For this study, the in situ observed U_{10} adjusted to U_{10EN} is identified as U_{10ENi} (section 1 and Table 1).

4.2. Fitting the Power Law

The data for both in situ U_{10} and adjusted in situ U_{10ENi} are used to derive the coefficients of the power law (1). The data are fit to the power law equation, not the log of the power law equation, in efforts to reduce bias associated with fitting the data in log space. The coefficients are chosen by minimizing the least squares error (LSE, defined as the sum of squared deviations of the fit from the observations), resulting in four sets of coefficients for a given wind speed range: a set of coefficients for each U_{10} and U_{10ENi} for W_i and a set of coefficients for each U_{10} and U_{10ENi} for W_{Ai}.

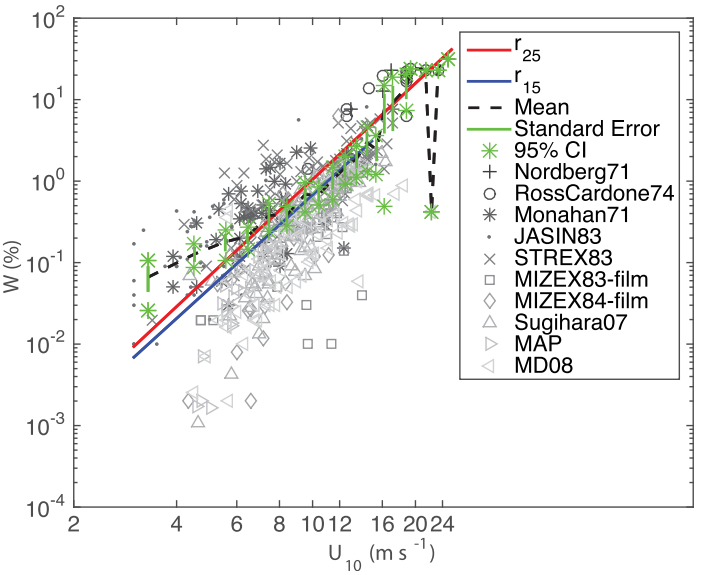

Figure 5. Whitecap fraction W as a function of wind speed U_{10} for wind speed ranges r_{25} (red solid line) and r_{15} (blue solid line) with mean of observations (black dashed line) and the standard error of W (green vertical lines).

Two wind speed ranges are considered: range r_{25} in which U_{10} or U_{10ENi} varies from 3 to about 25 m s^{-1}, and range r_{15} for winds of 3–15 m s^{-1}. The range r_{25} incorporates all the available data; the range r_{15} is chosen to avoid wind speeds with less than five observations in a wind speed bin. Consequentially, the range r_{15} incorporates nearly all of the early observations. The same ranges are applied to the WWD for comparison; the number of wind speed observations used in the WWD is sparse above 25 m s^{-1} and the uncertainty in the wind speeds above this range prohibits meaningful quantitative analysis of any results related to the in situ observations. *Callaghan et al.* [2008] and *Goddijn-Murphy et al.* [2011] identified improved parameterizations over low and high wind speed ranges using the MAP observations; however, to be consistent and comparable to the majority of the original parameterizations determined using the in situ and WWD data, continuous wind speed ranges are used in this study.

To identify how well the calculated parameterization represents the data, the observations are binned by wind speed in 1 m s^{-1} increments for the purpose of calculating the arithmetic mean, the standard error, and the 95% confidence intervals (CI). The standard error (or root-mean-square error) is calculated by dividing the standard deviation of the observations in each bin (i.e., $\sqrt{}$LSE) by the square-root of the number of observations in the bin. The 95% CI is calculated by multiplying the standard error by 1.96 [*Moore and McCabe*, 1999]. The means of the data, the magnitudes of standard error, and 95% CI are shown in Figures 5–8. An analysis of variance test is performed on the residuals of the whitecap parameterizations for the in situ data to determine changes in the mean and variance between parameterizations.

5. Results

Since U_{10} and U_{10ENi} describe different quantities, their relationships with W or W_A are not identical. The maximum difference between wind speeds U_{10} and U_{10ENi} associated with the W and W_A data sets is 2.45 and 1.15 m s^{-1}, respectively. The differences could be larger (or smaller) if currents and sea state were available (see section 4.1). Though these differences in U_{10} and U_{10ENi} might appear small, they are magnified when raised to a power. Therefore, these differences should be considered when using satellite-based winds for estimating whitecap fraction.

Coefficients to the power law are derived using both the W_A and W data sets over the two wind speed ranges r_{25} and r_{15} for both U_{10} and U_{10ENi}. Results for a total of eight coefficients pairs (a, b) are given in Table 3; the nonbolded rows are the results for the in situ wind speed U_{10} and the bolded rows are the results for the stability-adjusted in situ wind speed U_{10ENi} using the technique described in section 4.1. The change in the LSE from U_{10} to U_{10ENi} is provided as a measure of improvement: positive values indicate reduced error and improved fit of the function to the corresponding data.

5.1. Whitecap Parameterizations With In Situ U_{10}

For the W data set, the parameterization fits for the wind speed ranges 6–10 and 16–18 m s^{-1} for r_{25} and for the wind speed ranges 8–15 m s^{-1} for r_{15} are contained within the 95% CI of the data (Figure 5). Both fits perform very well at 9 m s^{-1} and higher. The r_{15} fit is within the standard error of the data from 9

Table 3. Coefficient Values From Power Law Fits for In Situ Observations for Whitecap Type (W and W_A in Percent), Wind Type (U_{10} and U_{10EN}), Range (r_{25} and r_{15}), and the Percentage Change in the LSE From U_{10} to U_{10EN}[a]

Whitecap	Wind	Range	a	b	LSE (%)
W	U_{10}	r_{25}	$1.26(3) \times 10^{-4}$	3.92	
W	**U_{10EN}**	**r_{25}**	**$1.72(8) \times 10^{-4}$**	**3.79**	**1.7**
W	U_{10}	r_{15}	$1.04(4) \times 10^{-4}$	3.81	
W	**U_{10EN}**	**r_{15}**	**$1.42(0) \times 10^{-4}$**	**3.69**	**−0.26**
W_A	U_{10}	r_{25}	$3.83(8) \times 10^{-4}$	3.07	
W_A	**U_{10EN}**	**r_{25}**	**$4.35(5) \times 10^{-4}$**	**3.01**	**1.7**
W_A	U_{10}	r_{15}	$4.19(9) \times 10^{-6}$	4.69	
W_A	**U_{10EN}**	**r_{15}**	**$2.89(5) \times 10^{-6}$**	**4.83**	**2**

[a]Bold identifies the stability-adjusted in situ wind speed U_{10EN} from the in situ wind speed U_{10}.

through 15 m s^{-1}. The r_{25} fit is close to the standard error above 9 m s^{-1} and captures W from the uppermost wind speed observations quite well. Both fits underestimate the observed W values for the 3–9 m s^{-1} range, which might point to different regimes for high and low wind speeds. The data points do not necessarily have a normal distribution; however, with the global locations of the data and the various analysis techniques used to determine the whitecap fraction, the parameterizations describe the data adequately.

For the W_A data set, the r_{15} fit is mostly contained within the standard error and the 95% CI of the data above 4 m s^{-1}, but the r_{25} fit is only contained at the bottom and top of the wind speed ranges (Figure 6). The r_{25} fit mostly overestimates the W_A values in the 3–10 m s^{-1} range, but is mostly within the standard error above 12 m s^{-1}. The r_{15} fit is mostly within the standard error above 5 m s^{-1}. It also closely follows the mean of the data. This result emphasizes the relatively heavy weight of the high wind speeds on the LSE with the parameterization optimized in real space instead of log space.

The power law exponent, coefficient b in Table 3 (nonbolded rows), for both cases of W_i and W_{Ai} in both ranges r_{25} and r_{15}, is from about 3 up to ~4.7. These values are similar to the coefficients found in the literature, ranging from 2 through 4 [*Anguelova and Webster*, 2006]. Most exponents approximate a cubic value, but exponents above 5 are reported, too [*Hanson and Phillips*, 1999]. Considering that the available data have fewer observations to fit at higher wind speeds, these fits are reasonable for W and W_A using U_{10}, with the caveat that the data sets do not show the true variability that would likely occur in nature.

One-way analysis of variance tests (ANOVA) are performed on the residuals of the whitecap parameterizations for both U_{10} and U_{10ENi}. For example, the residuals of the in situ observations and $W_i(U_{10ENi})$ are tested against the residuals of the in situ observations and $W_i(U_{10})$. This test is performed for $W_i(U_{10})$-W against $W_i(U_{10ENi})$-W and for $W_{Ai}(U_{10})$-W_A against $W_{Ai}(U_{10ENi})$-W_A for r_{25} and r_{15}. The tests are set up to determine if there is a significant change between two whitecap parameterizations representing the same in situ whitecap observations. For example, the residuals of the in situ observations and $W_i(U_{10ENi})$ are tested against the residuals of the in situ observations and $W_i(U_{10})$. The null hypothesis is that residuals from the two parameterizations being tested come from populations with the same mean; the null hypothesis is rejected with a p value

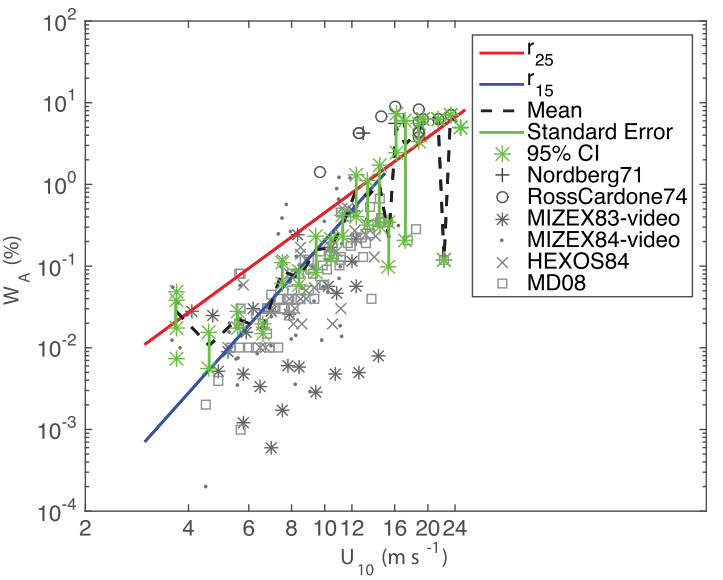

Figure 6. Same as Figure 5 except for W_A.

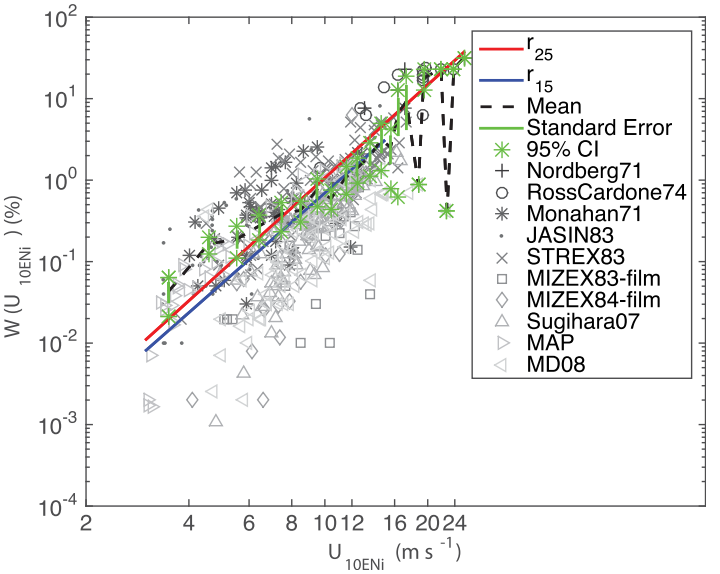

Figure 7. Same as Figure 5 except for U_{10EN}.

less than 0.05 for this test. None of the four tests rejected the null hypothesis with p values of 0.94 for the W_A r_{15} test and between 0.75 and 0.84 for the other three cases. These results are interpreted as the means and variances of the parameterizations using the different wind types are not significantly different, or they might be samples from the same distribution.

The LSE for $W_i(U_{10ENi})$ and $W_i(U_{10})$ results in 6.7% and 0.3% additional error for r_{25} and r_{15}, respectively. This error can be reduced if the parameterizations are optimized for U_{10ENi} instead. This in part confirms findings by *Goddijn-Murphy et al.* [2011] that parameterizations optimized for U_{10} and U_{10EN} to estimate whitecap coverage have different coefficients. However, for $W_{Ai}(U_{10})$ parameterizations, U_{10ENi} values reduced the error by 1.3% and 2.0% for r_{25} and r_{15}, respectively. While 2% might be within the margin of error given the nature of the data, a 6.7% increase in error encourages the utility of U_{10EN}-based parameterizations.

5.2. Whitecap Parameterizations With In Situ U_{10EN}

The power law fits $W_{ENi}(U_{10ENi})$ and $W_{AENi}(U_{10ENi})$ for ranges r_{25} and r_{15} are shown in Figures 7 and 8, respectively. Qualitatively, the overall trends for both $W_{ENi}(U_{10ENi})$ and $W_{AENi}(U_{10ENi})$ fits are the same as those in Figures 5 and 6 for the functional fits in terms of U_{10}. That is, the functions for both r_{25} and r_{15} capture the overall basic shape of the data, but fail to represent the mean of the data throughout the data ranges. The $W_{AENi}(U_{10ENi})$ for r_{15} is mostly within the 95% CI from 5–15 m s^{-1}, and above 11 m s^{-1} for r_{25}. Outside of those ranges, the fits are mostly poor. For the $W_{ENi}(U_{10ENi})$ fits, the mean is underestimated below 7 m s^{-1}; however, the fits are within the 95% CI above 7 m s^{-1}.

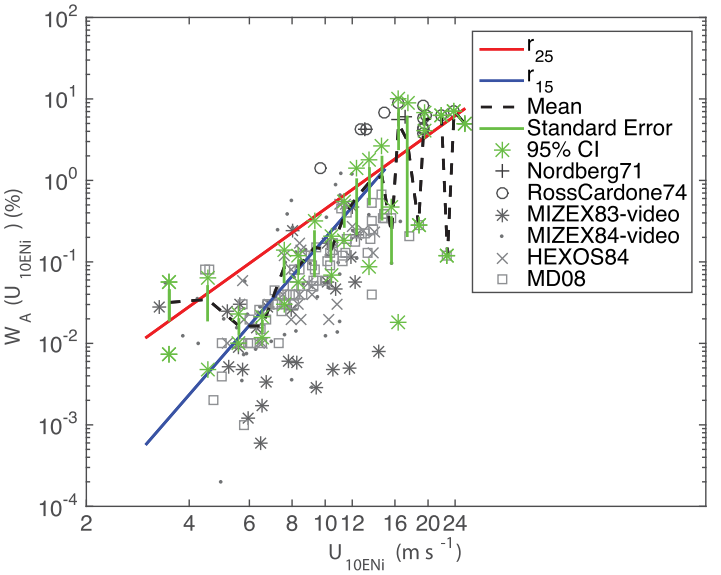

Figure 8. Same as Figure 6 except for U_{10EN}.

Quantitatively, however, the expected difference is confirmed (see the bolded rows in Table 3). Moreover, $W_{ENi}(U_{10ENi})$ and $W_{AENi}(U_{10ENi})$ estimate W and W_A at least as good as $W_i(U_{10})$ and $W_{Ai}(U_{10})$ according to the LSE for the given ranges. Therefore, the coefficients found for U_{10ENi} should be used when estimating W and W_A with U_{10ENi} winds to avoid introducing unnecessarily errors into the whitecap estimates.

One-way analysis of variance tests (ANOVA) are performed again on the residuals of the

whitecap parameterizations, but this test is performed for $W_i(U_{10})$-W against $W_{ENi}(U_{10ENi})$-W and for $W_{Ai}(U_{10})$-W_A against $W_{AENi}(U_{10ENi})$-W_A for r_{25} and r_{15}. None of the four tests rejected the null hypothesis with p values all above 0.91 and all above the previous tests. These results are interpreted as the means and variances of the parameterizations are not significantly different and they are less significantly different than using the mismatched wind type with the U_{10}-based parameterizations. The attempt to reduce the variance by accounting for stability in the wind profile does not prove statistically significant and the mean for the specified parameterization and correspond wind type remains statistically similar, indicating that the parameterizations perform equally well.

The derived coefficients are intended to be valid over their given ranges without extrapolation. Few observations exist at higher wind speeds making verification difficult. Additional observations and a calibration between the different techniques used for determining W and W_A would better help to determine the true mean and variance of the data and allow for better parameterizations capable of predicting W and W_A.

5.3. Whitecap Parameterizations With Satellite U_{10EN}

Ideally, the power law equations W_{ENi} and W_{AENi} should be able to predict the observed active and total whitecap fractions contained in the satellite-based WWD. The WWD provides wind and corresponding whitecap values for W_{37} and W_{10}; W_{37} is comparable to W, and W_{10} is comparable to W_A. The wind from the WWD (U_{10ENs}) is considered U_{10EN} and is directly used in the power law equation with the new coefficients appropriate for U_{10ENi} (bolded rows in Table 3), though some differences between U_{10ENs} and U_{10ENi} calculated from the in situ observations likely exist because of imperfect calibration between all platforms and wind sources involved.

For W_{37}, the in situ-based coefficients from the W fit are used over the ranges r_{25} and r_{15} (Figure 9). In situ observations are included to show differences with the satellite observations. At higher wind speeds, in situ observations far exceed the satellite observations. Because this feature is not observed for W_{10} (Figure 10), one cannot point to the sparseness of data at high winds as the sole reason for it. *Salisbury et al.* [2013] also noted this leveling off of W_{37} for winds above 20 m s^{-1} and suggested further investigation of this feature if it persists as the algorithm for satellite-based whitecap fraction is further developed. As with the in situ case, the coefficients for both r_{25} and r_{15} underestimate the mean value of W_{37} for $3 < U_{10ENs} < 12$ m s^{-1}. The r_{25} fit exponentially overestimates all values of W_{37} for $U_{10ENs} > 15$ m s^{-1}. The r_{15} fit resides within the W_{37} values close to 15 m s^{-1}, but would also exponentially overestimate W_{37} if extended to higher wind speeds. The change of the LSE from $W_i(U_{10ENs})$ and $W_{ENi}(U_{10ENs})$ shows an error reduction of 17% and 3% for r_{25} and r_{15}, respectively. This LSE improvement confirms that the U_{10EN}-based fits are more appropriate for W_{37} from the WWD; however, the fit is far from satisfactory for the WWD at higher wind speeds.

For W_{10}, the W_{Ai} and W_{AENi} parameterizations are used over the ranges r_{25} and r_{15} (Figure 10). The coefficients for both r_{25} and r_{15} underestimate the mean value of W_{10} for $3 < U_{10ENs} < 15$ m s^{-1}. In fact, the r_{15} fits for both $W_{Ai}(U_{10ENs})$ and $W_{AENi}(U_{10ENs})$ underestimate over 99.99% of the values of the W_{10}, but this is expected since the in situ values of W_A used to fit the parameterizations are smaller than W_{10} from WWD for U_{10ENs} at lower wind speeds. The r_{25} fit for both U_{10} and U_{10ENi} lie within W_{10} for $16 < U_{10EN} < 22$ m s^{-1} but overestimate for $U_{10EN} > 23$ m s^{-1}. The r_{25} fit for U_{10} overestimates W_{10} at lower wind speeds than the fit for U_{10EN}. The r_{25} fit performs remarkably well compared to the r_{15} fit, but still poorly estimates W_{10}. $W_{Ai}(U_{10ENs})$ show a marginal improvement of LSE over $W_{AENi}(U_{10ENs})$. This LSE increase does not discount the usefulness of W_{AENi}. Rather, $W_{Ai}(U_{10ENs})$ and $W_{AENi}(U_{10ENs})$ do not capture the mean W_{10} from the WWD. More appropriate coefficients for estimating W_{10} and W_{37}, independent of these in situ observations, can be found in *Salisbury et al.* [2013]. The ANOVA test is performed on the residuals of the whitecap parameterizations and all the corresponding values of W_{10} and W_{37} from the WWD for the given ranges; the null hypothesis is rejected in every case indicating that though differences in the parameterizations are statistically insignificant for the in situ cases, compared to the WWD and using U_{10ENs}, the differences in the parameterizations are statistically significant.

For both the W_A and the W cases, the actual in situ observations of the whitecap fraction with their corresponding U_{10} and U_{10ENi} at times vary orders of magnitude when compared to W_{10} and W_{37}. Additional geophysical parameters such as currents, swell, or orbital velocity, all necessary to account for surface motion when changing from an earth relative U_{10} to a surface relative U_{10EN}, might provide a partial explanation for these differences, but not all the differences. The errors in observations of U_{10} and dT also cannot contribute

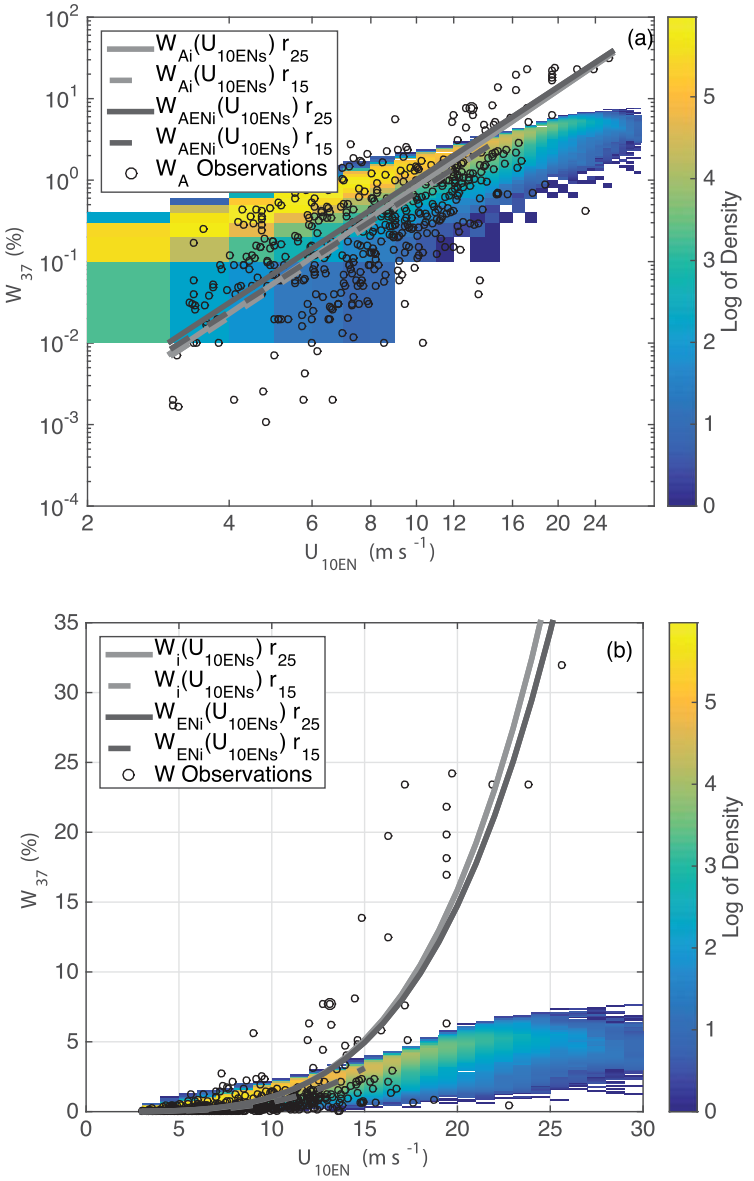

Figure 9. Density plot of W_{37} from WindSat Whitecap Database shown in the color rectangles; density of observations indicated by color-bar displayed in (a) log-scale and (b) linear scale. Observations W from the in situ data with the U_{10ENi} wind speeds are shown in black circles. Functional fits $W(U_{10ENs})$ (light gray) and $W_{ENi}(U_{10ENs})$ (dark gray) are shown for the ranges r_{25} (solid) and r_{15} (dashed).

enough to explain such differences, though accounting for surface conditions and any adjustments in the wind speed due to the observation height being different than 10 m [*May and Bourassa*, 2011] would also help explain the differences. Other geophysical parameters such as fetch and wind duration also have a notable effect on the sea-state and influence whitecap production. Another probable explanation is that the differences result from the techniques and the number of observations used to determine W and W_A. Additionally, the in situ observations rely on spatial resolution to resolve individual whitecaps to determine whitecap fraction, while radiometric observations rely on the observed brightness temperature from the observed total footprint to determine whitecap fraction. So the ability to resolve whitecap fraction and determine a relation between whitecap fraction and wind speed depends in part on the effective limit of the resolution of the observation and analysis techniques. The parameters that influence W, W_A, W_{10}, and W_{37}, such as sea spray in visible observations and the change-over point from active to residual whitecaps for both visible and microwave observations, also influence the coefficients and are a potential source of

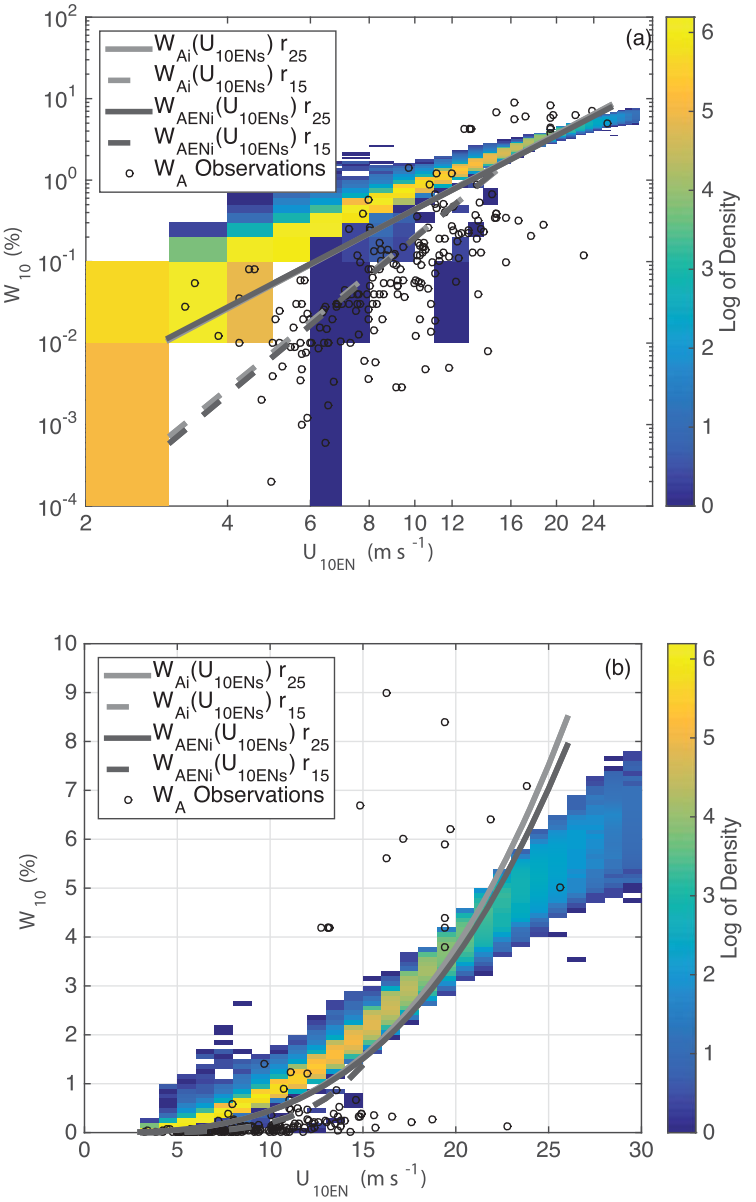

Figure 10. Density plot of W_{10} from WindSat Whitecap Database shown in the color rectangles; density of observations indicated by colorbar displayed in (a) log-scale and (b) linear scale. Observations W from the in situ data with the U_{10ENi} wind speeds are shown in black circles. Functional fits $W_A(U_{10ENs})$ (light gray) and $W_{AENi}(U_{10ENs})$ (dark gray) are shown for the ranges r_{25} (solid) and r_{15} (dashed).

differences. A calibration between techniques for determining whitecap fraction is merited in the future to help account for the unique biases but is not included as part of this research.

6. Conclusions

The differences between $W_{Ai}(U_{10})$ and $W_{AENi}(U_{10ENi})$ and between $W_i(U_{10})$ and $W_{ENi}(U_{10ENi})$ do not statistically significantly change the mean and variance of the residuals of the in situ observations. The similar LSE between parameterizations indicates that the parameterizations with the corresponding wind type and wind speed ranges estimate the in situ whitecaps used in this study equally well. Though the changes in the coefficients may appear small (Table 3), appropriate power law coefficients for the U_{10} or U_{10EN} reduce overall error for their respective parameterizations. Stability alone (required for changing U_{10} to U_{10EN}) does not statistically significantly account for the variability in the in situ whitecap observations and parameterizations. The parameterizations developed for the given wind speed ranges and types of wind are

recommended in general for both W and W_A for estimating in situ whitecap observations within the prescribed ranges. Still, previously published parameterizations might be more appropriate given similar local wind, wave, temperature, and stability conditions. Whitecap fraction estimates similar to the in situ W and W_A using U_{10EN} from satellites (e.g., QuikSCAT or ASCAT) is predicted better using the coefficients for $W_{ENi}(U_{10ENs})$ and $W_{AENi}(U_{10ENs})$ than $W_i(U_{10ENs})$ and $W_{Ai}(U_{10ENs})$. None of the parameterizations presented adequately estimate W_{37} or W_{10} over all ranges.

Updated coefficients and converted wind speeds alone do not account for discrepancies between in situ and satellite-based whitecap observations based on these parameterizations. When applied to the WindSat Whitecap Database (WWD), $W_{ENi}(U_{10ENs})$ and $W_i(U_{10ENs})$ predict W_{37} with limitations, while the coefficients for $W_{AENi}(U_{10ENs})$ and $W_{Ai}(U_{10ENs})$ should not be used to predict W_{10}. Better coefficients for $W_{10}(U_{10EN})$ and $W_{37}(U_{10EN})$ for estimating whitecap fraction from the WWD are available [*Salisbury et al*., 2014]. Additional factors such as fetch, sea surface temperature, wind duration, sea state, etc. need to be studied to help account for the variance of the whitecap observations.

The parameterizations do not adequately estimate W_{10} and W_{37} from the satellite-based WWD. The different techniques used to obtain W and W_A from the in situ observations possibly would benefit from calibration to the WWD to establish a common metric. The variability in both the actual whitecaps and the observational techniques used to calculate the whitecap fraction along with the accuracy in determining and recording the wind speed, T_s, and T_{air} might explain the differences between the WWD and the in situ observation values. The multiple analysis techniques of the in situ observations and the forward model used to determine the whitecap fraction from satellite observations in the WWD might also help explain some of the differences in the reported whitecap values. Additionally, the relationship between the temporal resolution of the in situ wind and spatial resolution of the satellite-based wind could introduce error in equating the winds. Until the differences are characterized and reconciled, discrepancies will continue to exist in local and global applications. The WWD provides sufficient observations from a single platform with a consistent estimating technique for determining local and global functions for W and W_A using satellite winds and other potentially influential parameters.

Acknowledgments

This work was supported by NOAA/COD and NASA OVWST. Magdalena D. Anguelova was supported by the Office of Naval Research, NRL Program element 61153N, work units WU 8967 and WU 4500. A. Callaghan provided the tabulated whitecap data with associated environmental conditions from the Marine Aerosol Production (MAP) campaign. All other data come from the references listed in Table 2. The data, including the calculated U_{10EN} values, are available in tabulated form from the corresponding author, A. Paget, at aaroncpaget@gmail.com. We appreciate the comments and suggestions by three anonymous reviewers.

References

Andreas, E. L., P. P. G. Persson, and J. E. Hare (2008), A bulk turbulent air-sea flux algorithm for high-wind, spray conditions, *J. Phys. Oceanogr.*, *38*, 1581–1596, doi:10.1175/2007JPO3813.1.

Anguelova, M. D., and P. W. Gaiser (2011), Skin depth at microwave frequencies of sea foam layers with vertical profile of void fraction, *J. Geophys. Res.*, *116*, C11002, doi:10.1029/2011JC007372.

Anguelova, M. D., and P. W. Gaiser (2013), Microwave emissivity of sea foam layers with vertically inhomogeneous dielectric properties, *Remote Sens. Environ.*, *139*, 81–96, doi:10.1016/j.rse.2013.07.017.

Anguelova, M. D., and F. Webster (2006), Whitecap coverage from satellite measurements: A first step toward modeling the variability of oceanic whitecaps, *J. Geophys. Res.*, *111*, C03017, doi:10.1029/2005JC003158.

Anguelova, M. D., M. Bettenhausen, and P. Gaiser (2006), Passive remote sensing of sea foam using physically-based models, in *International Geoscience and Remote Sensing Symposium*, pp. 3676–3679, Institute of Electrical and Electronics Engineers, doi:10.1109/IGARSS.2006.942.

Asher, W., Q. Wang, E. C. Monahan, and P. M. Smith (1998), Estimation of air-sea gas transfer velocities from apparent microwave brightness temperature, *J. Mar. Technol. Soc.*, *32*, 32–40.

Bartsch, A. (2010), Ten years of SeaWinds on QuikSCAT for snow applications, *Remote Sens.*, *2*, 1142–1156, doi:10.3390/rs2041142.

Bettenhausen, M., C. Smith, R. Bevilacqua, N. Wang, P. Gaiser, and S. Cox (2006), A nonlinear optimization algorithm for WindSat wind vector retrievals, *IEEE Trans. Geosci. Remote Sens.*, *44*(3), 597–610, doi:10.1109/TGRS.2005.862504.

Blanchard, D. (1963), The electrification of the atmosphere by particles from bubbles in the sea, *Prog. Oceanogr.*, *1*, 71–202.

Blanchard, D. (1983), The production, distribution and bacterial enrichment of the sea-salt aerosol, in *Air-Sea Exchange of Gases and Particles*, edited by P. Liss and G. Slinn, pp. 407–454, Springer, N. Y.

Bondur, V., and E. Sharkov (1982), Statistical properties of whitecaps on a rough sea, *Oceanology*, *22*, 274–279.

Callaghan, A. H. (2013), An improved whitecap model timescale for sea spray aerosol production flux modeling using the discrete whitecap method, *J. Geophys. Res. Atmos.*, *118*, 9997–10,010, doi:10.1002/jgrd.50768.

Callaghan, A. H., and M. White (2009), Automated processing of sea surface images for the determination of whitecap coverage, *J. Atmos. Oceanic Technol.*, *26*, 383–394, doi:10.1175/2008JTECHO634.1.

Callaghan, A. H., G. de Leeuw, L. Cohen, and C. D. O'Dowd (2008), Relationship of oceanic whitecap coverage to wind speed and wind history, *Geophys. Res. Lett.*, *35*, L23609, doi:10.1029/2008GL036165.

Callaghan, A. H., G. B. Deane, M. D. Stokes, and B. Ward (2012), Observed variation in the decay time of oceanic whitecap foam, *J. Geophys. Res.*, *117*, C09015, doi:10.1029/2012JC008147.

Chang, P. S., Z. Jelenak, J. M. Sienkiewicz, R. Knabb, M. J. Brennan, D. G. Long, and M. Freeberg (2009), Operational use and impact of satellite remotely sensed ocean surface vector winds in the marine warning and forecasting environment, *Oceanography*, *22*(2), 194–207.

Deane, G. B., and M. D. Stokes (2002), Scale dependence of bubble creation mechanisms in breaking waves, *Nature*, *418*, 839–844, doi:10.1038/nature00967.

de Leeuw, G., E. L. Andreas, M. D. Anguelova, C. W. Fairall, E. R. Lewis, C. O'Dowd, M. Schulz, and S. E. Schwartz (2011), Production flux of sea spray aerosol, *Rev. Geophys.*, *49*, RG2001, doi:10.1029/2010RG000349.
Doyle, D. (1984), Whitecaps and the marine atmosphere, *Rep. 6*, 140 pp., Univ. Coll., Galway, Ireland.
Gaiser, P. W., G. A. Poe, and W. L. Jones (2004), The WindSat spaceborne polarimetric microwave radiometer: Sensor description and early orbit performance, *IEEE Trans. Geosci. Remote Sens.*, *42*, 2347–2361.
Goddijn-Murphy, L., D. K. Woolf, and A. H. Callaghan (2011), Parameterizations and algorithms for oceanic whitecap coverage, *J. Phys. Oceanogr.*, *41*(4), 742–756, doi:10.1175/2010JPO4533.1.
Gordon, H. R., and K. J. Voss (1999), MODIS normalized water-leaving radiance algorithm theoretical basis document (MOD 18), Version 4, *Contract NAS5-31363*, Univ. of Miami, Coral Gables, Fla.
Gordon, H. R., and M. Wang (1994), Retrieval of water-leaving radiance and aerosol optical thickness over the oceans with SeaWiFS: A preliminary algorithm, *Appl. Opt.*, *33*, 443–452.
Hanson, J., and O. Phillips (1999), Wind sea growth and dissipation in the open ocean, *J. Phys. Oceanogr.*, *29*, 1633–1648.
Haywood, J. M., V. Ramaswamy, and B. J. Soden (1999), Tropospheric aerosol climate forcing in clear-sky satellite observations over the oceans, *Science*, *283*(5406), 1299–1303, doi:10.1126/science.283.5406.1299.
Ichoku, C., D. A. Chu, S. Mattoo, Y. J. Kaufman, L. A. Remer, D. Tanré, I. Slutsker, and B. Holben (2002), A spatio-temporal approach for global validation and analysis of MODIS aerosol products, *Geophys. Res. Lett.*, *29*(12), 1616, doi:10.1029/2001GL013206.
Kara, A. B., H. E. Hurlburt, and A. J. Wallcraft (2005), Stability-dependent exchange coefficients for air–sea fluxes, *J. Atmos. Oceanic Technol.*, *22*, 1080–1094.
Kara, A. B., A. J. Wallcraft, and M. A. Bourassa (2008), Air-sea stability effects on the 10 m winds over the global ocean: Evaluations of air-sea flux algorithms, *J. Geophys. Res.*, *113*, C04009, doi:10.1029/2007JC004324.
Kleiss, J. M., and W. Melville (2011), The analysis of sea surface imagery for whitecap kinematics, *J. Atmos. Oceanic Technol.*, *28*(2), 219–243, doi:10.1175/2010JTECHO744.1.
Lafon, C., J. Piazzola, P. Forget, O. le Calve, and S. Despiau (2004), Analysis of the variations of the whitecap fraction as measured in a coastal zone, *Boundary Layer Meteorol.*, *111*, 339–360, doi:10.1023/B:BOUN.0000016490.83880.63.
Lafon, C., J. Piazzola, P. Forget, and S. Despiau (2007), Whitecap coverage in coastal environment for steady and unsteady wave field conditions, *J. Mar. Syst.*, *66*, 38–46, doi:10.1016/j.jmarsys.2006.02.013.
Lewis, E., and S. Schwartz (2004), *Sea Salt Aerosol Production: Mechanisms, Methods, Measurements and Models: A Critical Review, Geophys. Monogr. Ser.*, vol. 152, Washington, D. C., doi:10.1029/GM152.
Lungu, T., and P. S. Callahan (2006), *QuikSCAT Science Data Product User's Manual: Overview and Geophysical Data Products*, Version 3.0, D-18053–RevA, Jet Propul. Lab., Calif. Inst. of Technol., Pasadena. [Available at ftp://podaac.jpl.nasa.gov/allData/quikscat/L2B12/docs/QSUG_v3.pdf.]
May, J., and M. A. Bourassa (2011), Quantifying variance due to temporal and spatial difference between ship and satellite winds, *J. Geophys. Res.*, *116*, C08013, doi:10.1029/2010JC006931.
Melville, W. K. (1996), The role of surface-wave breaking in air-sea interaction, *Annu. Rev. Fluid Mech.*, *28*, 279–321.
Melville, W. K., and P. Matusov (2002), Distribution of breaking waves at the ocean surface, *Nature*, *417*, 58–63, doi:10.1038/417058a.
Memery, L., and L. Merlivat (1985), Modeling of gas flux through bubbles at the air-water interface, *Tellus, Ser. B*, *34*, 212–285.
Mironov, A. S., and V. A. Dulov (2008), Detection of wave breaking using sea surface video records, *Meas. Sci. Technol.*, *19*, 015405, 1–5, doi:10.1088/0957-0233/19/1/015405..
Monahan, E. (1971), Oceanic whitecaps, *J. Phys. Oceanogr.*, *1*, 139–144.
Monahan, E. (1993), Occurrence and evolution of acoustically relevant subsurface bubble plumes and their associated, remotely monitorable, surface whitecaps, in *Natural Physical Sources of Underwater Sound*, edited by B. Kerman, pp. 503–517, Springer, N. Y.
Monahan, E., and I. G. O'Muircheartaigh (1980), Optimal power-law description of oceanic whitecap coverage dependence on wind speed, *J. Phys. Oceanogr.*, *10*, 2094–2099.
Monahan, E., and I. G. O'Muircheartaigh (1982), Reply (to comments of J. *Wu* on (Optimal power-law description of oceanic whitecap coverage dependence on wind speed"), *J. Phys. Oceanogr.*, *12*, 751–752.
Monahan, E., and I. O'Muircheartaigh (1986), Whitecaps and the passive remote sensing of the ocean surface, *Int. J. Remote Sens.*, *7*, 627–642.
Monahan, E., and I. G. O'Muircheartaigh (2012), Oceanic whitecaps and the 10m-elevation wind speed: Toward improved power-law descriptions for use in climate modeling, paper presented at 18th Air-Sea Interaction Conference, Amer. Meteorol. Soc., Boston, Mass., 19–13 Jul.
Monahan, E., and D. Woolf (1989), Comments on "Variations of whitecap coverage with wind stress and water temperature," *J. Phys. Oceanogr.*, *19*, 706–709.
Monahan, E., M. Spillane, P. Bowyer, D. Doyle, and P. Stabeno (1983), Whitecaps and the marine atmosphere, *Rep. 5*, 93 pp., Univ. Coll., Galway, Ireland.
Monahan, E., M. Spillane, P. Bowyer, M. Higgins, and P. Stabeno (1984), Whitecaps and the marine atmosphere, *Rep. 7*, 103 pp., Univ. Coll., Galway, Ireland.
Monahan, E., P. Bowyer, D. Doyle, M. Higgins, and D. Woolf (1985), Whitecaps and the marine atmosphere, *Rep. 8*, 124 pp., Univ. Coll., Galway, Ireland.
Moore, D. S., and G. P. McCabe (1999), *Introduction to the Practice of Statistics*, 3rd ed., 825 pp., W. H. Freeman, N. Y.
Nordberg, W., J. Conaway, D. Ross, and T. Wilheit (1971), Measurements of microwave emission from a foam-covered, wind-driven sea, *J. Atmos. Sci.*, *28*, 429–435.
Plagge, A. M., D. Vandemark, and B. Chapron (2012), Examining the impact of surface currents on satellite scatterometer and altimeter ocean winds, *J. Atmos. Oceanic Technol.*, *29*, 1776–1793, doi:10.1175/JTECH-D-12-00017.1.
Powell, M. D., P. J. Vickery, and T. A. Reinhold (2003), Reduced drag coefficients for high wind speeds in tropical cyclones, *Nature*, *422*, 279–283.
Rose, L., W. Asher, S. Reising, P. Gaiser, K. St Germain, D. Dowgiallo, K. Horgan, G. Farquharson, and E. Knapp (2002), Radiometric measurements of the microwave emissivity of foam, *IEEE Trans. Geosci. Remote Sens.*, *40*(12), 2619–2625, doi:10.1109/TGRS.2002.807006.
Ross, D., and V. Cardone (1974), Observations of oceanic whitecaps and their relation to remote measurements of surface wind speed, *J. Geophys. Res.*, *79*, 444–452.
Salisbury, D. J., M. D. Anguelova, and I. M. Brooks (2013), On the variability of whitecap fraction using satellite-based observations, *J. Geophys. Res. Oceans*, *118*, 6201–6222, doi:10.1002/2013JC008797.

Salisbury, D. J., M. D. Anguelova, and I. M. Brooks (2014), Global distribution and seasonal dependence of satellite-based whitecap fraction, *Geophys. Res. Lett.*, *41*, 1616–1623, doi:10.1002/2014GL059246.
Smith, P. (1988), The emissivity of sea foam at 19 and 37 GHz, *IEEE Trans. Geosci. Remote Sens.*, *26*, 541–547.
Stramska, M., and T. Petelski (2003), Observations of oceanic whitecaps in the north polar waters of the Atlantic, *J. Geophys. Res.*, *108*, 3086, doi:10.1029/2002JC001321, C3.
Sugihara, Y., H. Tsumori, T. Ohga, H. Yoshioka, and S. Serizawa (2007), Variation of whitecap coverage with wave-field conditions, *J. Mar. Syst.*, *66*, 47–60.
Tang, W., and W. T. Liu (1996), Equivalent neutral wind, *Rep. 96-17*, Jet Propul. Lab., Calif. Inst. of Technol., Pasadena.
Taylor, G. I. (1938), The spectrum of turbulence, *Proc. R. Soc. London, Ser. A*, *67*, 16–20.
Thorpe, S. A. (1982), On the clouds of bubbles formed by breaking wind-waves in deep water, and their role in air-sea gas transfer, *J. Philos. Trans. R. Soc. London, Ser. A*, *304*, 155–216.
Wentz, F. (1983), A model function for ocean microwave brightness temperature, *J. Geophys. Res.*, *88*, 1892–1908.
Wentz, F. (1997), A well-calibrated ocean algorithm for special sensor microwave/imager, *J. Geophys. Res.*, *102*, 8703–8718.
Wilheit, T. (1979), A model for the microwave emissivity of the ocean's surface as a function of wind speed, *IEEE Trans. Geosci. Electron.*, *17*, 244–249.
Williams, G., Jr. (1969), Microwave radiometry of he ocean and eh possibility of marine wind velocity determination from satellite observations, *J. Geophys. Res.*, *18*, 4591–4594.
Woolf, D. (1997), Bubbles and their role in gas exchange, in *The Sea Surface and Global Change*, vol. 10, edited by P. S. Liss and R. A. Duce, pp. 173–205, Cambridge Univ. Press, Cambridge, U. K., doi:10.1017/CBO9780511525025.007.
Woolf, D. K., and S. A. Thorpe (1991), Bubbles and the air-sea exchange of gasses in near-saturation conditions, *J. Mar. Res.*, *49*, 435–466.
Wu, J. (1979), Oceanic whitecaps and sea state, *J. Phys. Oceanogr.*, *9*, 1064–1068.
Wu, J. (1988), Variations of whitecap coverage with wind stress and water temperature, *J. Phys. Oceanogr.*, *18*, 1448–1453.
Wu, J. (1992), Individual characteristics of whitecaps and volumetric description of bubbles, *IEEE Trans. Oceanic Eng.*, *17*, 150–158.